IEEE Access
Multidisciplinary ⋮ Rapid Review ⋮ Open Access Journal

Received 17 April 2023, accepted 14 May 2023, date of publication 18 May 2023, date of current version 24 May 2023.

Digital Object Identifier 10.1109/ACCESS.2023.3277622

RESEARCH ARTICLE

Multi-Disturbance Factors Analysis and Suppression Strategy of Sub-Synchronous Oscillation on DFIG Grid-Side Converter

DONGYANG SUN, WENQIANG SHEN, ZIJIE QIAN, FANYI MENG, YUTONG SHA, AND KAI ZHOU

College of Electrical and Electronic Engineering, Harbin University of Science and Technology, Harbin 150080, China

Corresponding author: Wenqiang Shen (2120310243@stu.hrbust.edu.cn)

This work was supported in part by the Heilongjiang Provincial Natural Science Foundation of China under Grant LH2021E086.

ABSTRACT This paper focuses on the power grid oscillation of grid-side converter (GSC) in doubly-fed induction generator (DFIG) caused by grid sub-synchronous oscillation (SSO), and designs a measure to improve the output power quality of GSC. Firstly, the influence mechanism of multipath disturbance of GSC under SSO is sorted out, and the disturbance factors and action modes are clarified. Secondly, the influence of SSO on the output estimation of phase-locked loop (PLL) in the control strategy and power calculation process is analyzed. Furthermore, the mathematical model of GSC output power considering the influence of PLL is established. At the same time, the key factors of SSO for GSC power oscillation suppression strategy are determined by analyzing the oscillation suppression effect of quasi-resonant controller when SSO amplitude, frequency and phase change. Based on the above theoretical analysis and research, the resonant controller is used to eliminate the estimation error of the PLL; at the same time, an adaptive algorithm is designed according to the mechanism analysis of SSO characteristic changes to improve the fixed resonant frequency of the quasi-resonant controller, and a DFIG-GSC sub-synchronous power oscillation suppression strategy based on the adaptive quasi-resonant controller is proposed, thus eliminating the influence of SSO on the multipath disturbance of GSC and improving the power quality of its output. Finally, the effectiveness of the proposed suppression strategy is verified by simulation and experimental results.

INDEX TERMS Power quality, doubly-fed induction generator (DFIG), grid side converter (GSC), phase locked loop (PLL), sub-synchronous oscillation frequency change, adaptive quasi-resonant controller.

I. INTRODUCTION

The rapid development of new energy technology has further increased the installed capacity of wind power. Doubly-fed induction generator (DFIG) has been widely used in the field of wind power generation because of its small converter capacity and variable speed constant frequency power generation [1]. However, a large number of static Var compensators and series compensation capacitors are connected to the power grid in the process of UHV power transmission, resulting in sub-synchronous oscillation (SSO) and power quality decline [2], [3], [4]. Power grid SSO will affect the stability of wind power generation, which will lead to wind turbine off-grid, thermal power and other generator tripping accidents [5], [6], [7], [8]. In 2009, a SSO accident occurred in the United States, resulting in an urgent abandonment of the wind [5]. Since 2010, there have been more than ten SSO accidents with oscillation frequency between 4∼8 Hz in North China [6]; there have also been many SSO accidents in the northwest region, and the oscillation frequency is in the range of 10∼20 Hz, resulting in the shutdown of thermal power units hundreds of kilometers away from the wind farm [7]. In 2019, a SSO accident occurred at the Horn wind farm in the UK, resulting in a loss of 3.2% of the load, affecting about 1 million users [8].

Researches have shown that SSO has complex mechanism, fuzzy transient model, various types and wide-area propagation characteristics [9], [10]. The reference [10] introduces

The associate editor coordinating the review of this manuscript and approving it for publication was R.K. Saket.

This work is licensed under a Creative Commons Attribution-NonCommercial-NoDerivatives 4.0 License.
For more information, see https://creativecommons.org/licenses/by-nc-nd/4.0/

the evolution of SSO in the grid and the classification of existing forms, and the new SSO problem characterized by the interaction between converter and power grid in recent years were studied. After the SSO generated by any reason is input into the wind turbine, the fault form is to cause the power oscillation of the unit output, which will cause the power quality of the power grid to decrease. Therefore, it is necessary to design a corresponding power oscillation suppression strategy.

As an important part of the DFIG unit, the grid side converter (GSC) is directly connected to the grid and has an important impact on the power quality of the power grid [11], [12]. Most scholars focus on the transmission of oscillation power between GSC in DFIG unit and power grid under the condition of high harmonics of grid voltage, which affects the power quality of power grid [13], [14], [15], [16], [17]. In reference [13], aiming at the problem of miscontrol of GSC in the case of harmonics in the power grid, notch filter is adopted to improve the GSC control strategy, so as to make it output stable active power and improve the power quality of GSC output. Reference [14] analyzed the influence of higher harmonics on the output power of GSC system by establishing a mathematical model, and proposed the resonant sliding mode algorithm to improve the control strategy of GSC system and suppress the power oscillation of GSC. However, these methods rely on the precise modeling of DFIG and are very sensitive to the parameters of the motor, which may vary during the operation of the motor. Reference [15] propose a direct power control (DPC) strategy based on quasi-resonance to suppress the pulsation component in the output power of GSC by analyzing the working state of GSC under the condition of harmonic voltage in the power grid. References [16] and [17] analyze the influence of double frequency generated by negative sequence component on GSC, and proposed the method of model predictive control to improve the robustness of GSC system, so as to improve the power quality of the system output. However, this kind of fuzzy control method is not mature enough, and the design process is more complex, it needs a lot of existing data to fully predict it. At present, there are few researches on the output power quality of GSC in SSO state of power grid. In reference [18], linear extended state observer is used to improve the traditional static reactive power compensator, so as to realize the estimation and compensation of sub-synchronous components, and then suppress the influence of external sub-synchronous disturbance components on GSC power. In reference [19], SSO damping controller was added to GSC double closed loop and feedforward compensation loop respectively. By analyzing the running state under different conditions, it was concluded that adding damping controller to the current inner loop could obtain the optimal power oscillation suppression effect. References [20] and [21] studied the additional damping control strategy in the GSC control strategy to reduce the output oscillation power of GSC. Common SSO suppression strategies are listed in Table 1.

TABLE 1. Common SSO suppression strategies.

Suppression means	Concrete method	Characteristic
Additional damping control for wind turbine	Additional damping	Occupying the converter capacity of wind turbine
Series FACTS	gate level control series capacitor (GCSC), static synchronous series compensator (SSSC), etc.	Poor flexibility and investment is large
Parallel FACTS	Static reactive power compensator (SVC), static synchronous compensator (STATCOM), etc.	The inhibition capacity is related to the device capacity
Change the system running mode	Avoid the point where SSO occurs	It is difficult to establish electromagnetic transient model
Cut out the line complement capacitance	Cut out the line complement capacitance	Frequent switching damages the power grid
Parameter optimization and improved control strategy of controller	Optimize the controller parameters and control strategy	Limited inhibitory capacity

References [22] and [23] showed that SSO in DFIG is jointly affected by many factors such as power generation parameters and power grid parameters, so SSO characteristics are different under different operating conditions. The existing control strategy has the disadvantages of complex design and low adaptability, which can't well meet the suppression requirements under the change of SSO characteristics. At the same time, according to the analysis in this paper, the disturbance generated by the grid SSO on the GSC is not unique, including the influence of the oscillation power output of the GSC on the grid, but also the influence of the SSO voltage on the estimated value of the Phase-locked loop (PLL), so the corresponding oscillation suppression measures should be taken.

Based on the above problems, this paper focuses on the research of suppressing the oscillating power of GSC in SSO state. Firstly, the disturbance mode of power grid SSO in GSC system is analyzed. Secondly, the influence of SSO on PLL is analyzed, and the function relationship of GSC power with PLL influence in SSO state is established. At the same time, the influence of SSO characteristics on the suppression strategy of GSC power oscillation is analyzed. Furthermore, an improved PLL using resonant controller is designed to improve the accuracy of PLL output. At the same time, an improved control strategy of GSC based on adaptive quasi-resonant controller is designed to realize the suppression of GSC oscillation power. Finally, a DFIG system vibration suppression simulation model and experimental platform were built to verify the effectiveness of the proposed oscillation suppression strategy.

II. MECHANISM ANALYSIS OF MULTIPLE DISTURBANCE FACTORS OF POWER GRID SSO TO GSC

A. ANALYSIS OF INFLUENCE OF GRID SSO ON GSC WITHOUT PLL PHASE ERROR

Without counting the PLL output error, if SSO frequency is ω_{sso}, the expression of grid side voltage in d-q coordinate system is shown in (1):

$$\begin{cases} u_{gd} = u_{gd0} + u_{gdsso} \\ = U_g + U_{sso}\cos[(\omega_1 - \omega_{sso})t + \varphi_{usso}] \\ u_{gq} = u_{gq0} + u_{gqsub} \\ = 0 + U_{sso}\sin[(\omega_1 - \omega_{sso})t + \varphi_{usso}] \end{cases} \tag{1}$$

In (1), U_g and U_{sso} are the amplitudes of power grid fundamental wave voltage and SSO voltage vector respectively; ω_1 is the angular velocity of the fundamental wave voltage of the grid; φ_{usso} is the initial phase angle of grid SSO voltage in d-q coordinate system.

Similarly, the current at the GSC can be expressed in the d-q coordinate system as:

$$\begin{cases} i_{gd} = i_{gd0} + i_{gdsso} \\ = I_g + I_{sso}\cos[(\omega_1 - \omega_{sso})t + \varphi_{isso}] \\ i_{gq} = i_{gq0} + i_{gqsso} \\ = 0 + I_{sso}\sin[(\omega_1 - \omega_{sso})t + \varphi_{isso}] \end{cases} \tag{2}$$

In (2), I_g and I_{sso} are the amplitudes of ideal current and SSO current vectors; φ_{isso} is the initial phase angle of SSO current in the d-q coordinate system.

By combining (1) and (2), the active power expression of GSC system can be obtained as shown in (3):

$$\begin{aligned} P_g &= -\frac{3}{2}(u^*_{gd}i_{gd} + u^*_{gq}i_{gq}) \\ &= -\frac{3}{2}[(u_{gd0} + u_{gdsso})^*(i_{gd0} + i_{gdsso}) + u^*_{gqsso}i_{gqsso}] \\ &= -\frac{3}{2}\begin{pmatrix} U_gI_g + \\ U_{sso}I_{sso}\cos(\varphi_{usso} - \varphi_{isso}) + \\ U_{sso}I_g\cos[(\omega_1 - \omega_{sso})t + \varphi_{usso}] + \\ U_gI_{sso}\cos[(\omega_1 - \omega_{sso})t + \varphi_{isso}] \end{pmatrix} \end{aligned} \tag{3}$$

Similarly, the reactive power of GSC system can be expressed as:

$$\begin{aligned} Q_g &= -\frac{3}{2}(u^*_{gq}i_{gd} - u^*_{gd}i_{gq}) \\ &= -\frac{3}{2}[u^*_{gqsso}(i_{gd0} + i_{gdsso}) - (u_{gd0} + u_{gdsso})^*i_{gqsso}] \\ &= -\frac{3}{2}\begin{pmatrix} U_{sso}I_{sso}\sin(\varphi_{usso} - \varphi_{isso}) + \\ U_{sso}I_g\sin[(\omega_1 - \omega_{sso})t + \varphi_{usso}] - \\ U_gI_{sso}\sin[(\omega_1 - \omega_{sso})t + \varphi_{isso}] \end{pmatrix} \end{aligned} \tag{4}$$

Equations (3) and (4) are GSC power expressions without considering PLL output error when SSO occurs in the power grid. However, under the influence of grid SSO, in practical engineering, GSC system will be affected by PLL output error when calculating power, and the control strategy of GSC will also be interfered by PLL output error. Therefore, it is necessary to establish a more accurate mathematical model of the output power of GSC system considering the influence of PLL.

B. INFLUENCE ANALYSIS OF GRID SSO WITH PLL OUTPUT ERROR ON GSC

In the SSO state of power grid, the control effect of PLL will be interfered, affecting the control strategy of GSC system and the calculation process of GSC power. It will make the process of control strategy and power calculation more complicated. The multi-input disturbance diagram of GSC system under SSO state of power grid is shown in Fig. 1.

In Fig. 1, C is the dc bus support capacitance; V_{dc} represents dc bus voltage; I_{load} indicates the load current; U_{ga0}, U_{gb0}, U_{gc0}, and I_{ga0}, I_{gb0}, and I_{gc0} represent the three-phase voltage and current of the power grid respectively; U_{gasso}, U_{gbsso}, U_{gcsso} and I_{gasso}, I_{gbsso} and I_{gcsso} respectively represent the sub-synchronous voltage and sub-synchronous current components of the grid; R and L represent filter resistance and inductance respectively; θ_1 is the phase of the ideal grid voltage; $\delta\theta$ is the error between pll output voltage phase and ideal voltage phase in sso state.

As shown in Fig. 1, power grid sso has input characteristics of multi-disturbance factors to gsc, including error signal generates by pll, current disturbances in actual converter, and coupling effects between them. Specific analysis are as follows:

The signal disturbance is the pll output error in the sso state of the power grid, in which the phase signal with the error has an impact on the coordinate transformation process of the gsc control system, and it is difficult to lock the signal of the power grid fundamental wave voltage, which causes the feedforward decoupling compensation term in the gsc control strategy to oscillate.

The physical quantity disturbance is the current disturbance in the actual converter, and the grid side current oscillation will cause the dc component of the converter to oscillate in the d-q coordinate system.

At the same time, the grid-side current disturbance caused by the coupling of pll output error signal and converter current oscillation is superimposed with grid-side oscillation current caused by grid sso, which aggravates the complexity of gsc output power oscillation.

Therefore, pll will be improved later in this paper to ensure the accuracy of its output phase, voltage amplitude and frequency estimates. At the same time, by improving the control strategy of gsc, the output power stability of the system is improved.

C. INFLUENCE ANALYSIS OF GRID SSO WITH PLL OUTPUT ERROR ON GSC

Synchronous reference frame-phase-locked loop (srf-pll) is commonly used in grid-connected systems. in order to analyze the influence of grid sso on gsc under the influence of pll phase error, the srf-pll mathematical model in the case of grid sso should first be established. The block diagram of srf-pll in the case of grid sso is shown in Fig. 2.

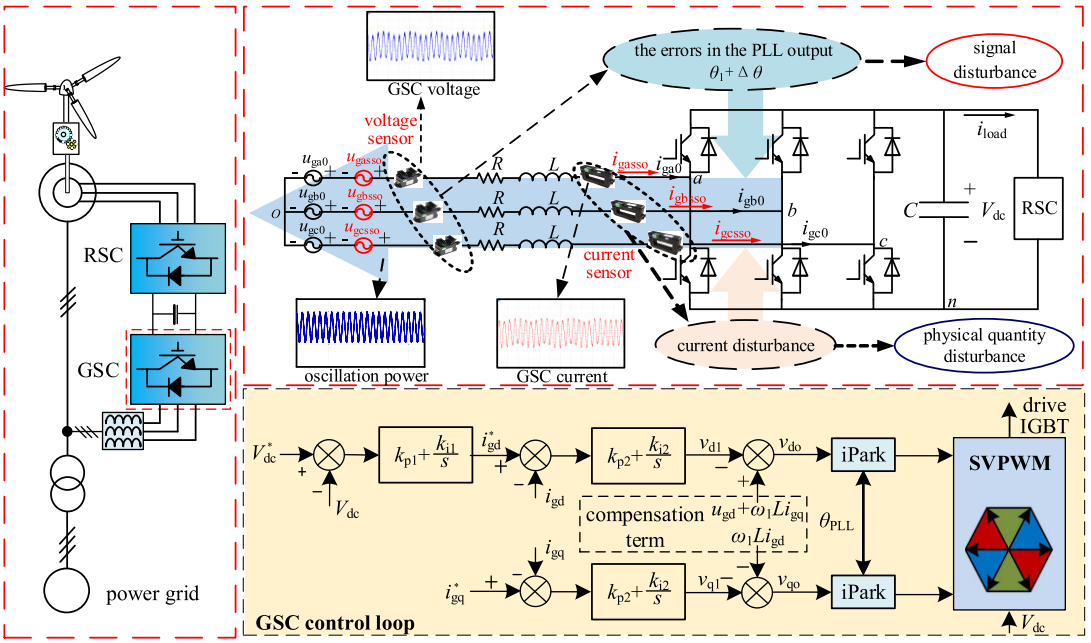

FIGURE 1. Diagram of multi-disturbance factors of GSC system in SSO state of power grid.

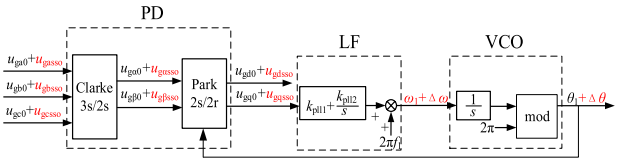

FIGURE 2. SRF-PLL block diagram in SSO state of power grid.

It can be seen from (1) that the grid voltage all contains AC components in the d-q coordinate system. According to Fig. 2, q-axis component is used for closed-loop control, and the transfer function of loop filter is assumed to be:

$$G_1(s) = k_{\text{pll1}} + \frac{k_{\text{pll2}}}{s} \tag{5}$$

after passing through the loop filter, the oscillation component of the Q-AXIS can be expressed as:

$$\begin{aligned}\Delta\omega &= U_{\text{sso}} k_{\text{pll1}} \sin\left[(\omega_{\text{sso}} - \omega_1)\, t + (\varphi_{\text{usso}} - \varphi_1)\right] \\ &\quad + U_{\text{sso}} k_{\text{pll2}} \int \sin\left[(\omega_{\text{sso}} - \omega_1)\, t + (\varphi_{\text{usso}} - \varphi_1)\right] dt \\ &= a \sin\left[(\omega_{\text{sso}} - \omega_1)\, t \right. \\ &\quad \left. + \left(\varphi_{\text{usso}} - \varphi_1 - \arctan \frac{k_{\text{pll2}}}{k_{\text{pll1}}\,(\omega_{\text{sso}} - \omega_1)}\right)\right]\end{aligned} \tag{6}$$

In (6), $a = U_{\text{sso}} \sqrt{k_{\text{pll1}}^2 + \left(\frac{k_{\text{pll2}}}{\omega_{\text{sso}} - \omega_1}\right)^2}$.

at this time, the output error phase of the voltage-controlled oscillator is:

$$\begin{aligned}\Delta\theta &= a \int \sin\left[(\omega_{\text{sso}} - \omega_1)\, t \right. \\ &\quad \left. + \left(\varphi_{\text{usso}} - \varphi_1 - \arctan \frac{k_{\text{pll2}}}{k_{\text{pll1}}\,(\omega_{\text{sso}} - \omega_1)}\right)\right] dt \,\%\, (2\pi) \\ &= -\frac{a}{(\omega_{\text{sso}} - \omega_1)} \cos\left[(\omega_{\text{sso}} - \omega_1)\, t \right. \\ &\quad \left. + \left(\varphi_{\text{usso}} - \varphi_1 - \arctan \frac{k_{\text{pll2}}}{k_{\text{pll1}}\,(\omega_{\text{sso}} - \omega_1)}\right)\right] \%\, (2\pi)\end{aligned} \tag{7}$$

In order to explore the influence of grid SSO on PLL output angular velocity and phase estimation, relevant simulation analysis is carried out. In the simulation process, the power grid fundamental wave voltage amplitude is 690 V, frequency is 50 Hz, SSO voltage amplitude is 138 V (20% of the fundamental wave voltage), frequency ω_{sso} is 20 Hz.

Fig. 3(a) is the estimated value ω_{PLL} of PLL output angular velocity in the SSO state of the grid, which including the oscillation component with frequency $\omega_1 - \omega_{\text{sso}}$. Fig. 3(b) is the estimated value of PLL output phase θ_{PLL} in SSO state of the power grid. It can be seen from the Fig. 3(b) that there is also error disturbance in the estimated value of phase, which damages the stability of the control strategy.

It can be seen from (7) that the phase output of PLL contains periodic oscillation component, which further affects the angle required by park transformation.

Considering the influence of oscillation voltage at the junction point on PLL, the output phase θ_{PLL} can be expressed

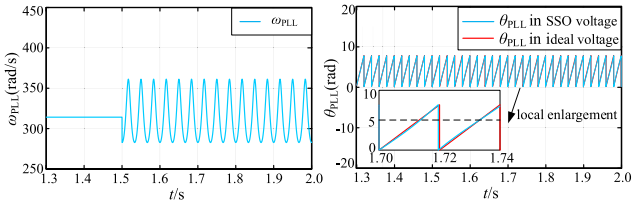

(a) PLL output electric angular velocity estimate (b) PLL output phase estimate

FIGURE 3. Estimated angular velocity and phase of PLL output in grid SSO state.

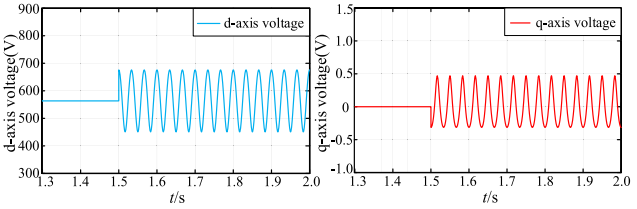

(a) PLL output d-axis component (b) PLL output q-axis component

FIGURE 4. PLL output estimation voltage under grid SSO state.

by (8):

$$\theta_{\mathrm{PLL}}(t) = \theta_1(t) + \Delta\theta(t) \tag{8}$$

In (8), $\theta_1(t)$ represents the phase of the fundamental voltage of the dot junction. $\Delta\theta(t)$ represents the phase disturbance component corresponding to the SSO voltage of the dot alignment.

According to the coordinate transformation Angle θ_{PLL} obtained by the PLL, the corresponding Park transformation matrix can be expressed as:

$$T_{2s/2r(\theta_{\mathrm{PLL}})} = \begin{bmatrix} \cos\theta_{\mathrm{PLL}} & \sin\theta_{\mathrm{PLL}} \\ -\sin\theta_{\mathrm{PLL}} & \cos\theta_{\mathrm{PLL}} \end{bmatrix} \tag{9}$$

In (9), the expression of $\cos\theta_{\mathrm{PLL}}$ and $\sin\theta_{\mathrm{PLL}}$ is:

$$\begin{cases} \cos\theta_{\mathrm{PLL}} = \cos\theta_1\cos\Delta\theta - \sin\theta_1\sin\Delta\theta \\ \approx \cos\theta_1 - \Delta\theta\sin\theta_1 \\ \sin\theta_{\mathrm{PLL}} = \sin\theta_1\cos\Delta\theta + \cos\theta_1\sin\Delta\theta \\ \approx \sin\theta_1 + \Delta\theta\cos\theta_1 \end{cases} \tag{10}$$

By substituting (10) into (9) and linearizing, the Park transformation matrix under SSO state of power grid can be obtained as [24]:

$$\begin{aligned} T_{2s/2r(\theta_{\mathrm{PLL}})} &= T_{2s/2r(\Delta\theta)} \cdot T_{2s/2r(\theta_1)} \\ &\approx \begin{bmatrix} 1 & \Delta\theta \\ -\Delta\theta & 1 \end{bmatrix} \cdot \begin{bmatrix} \cos\theta_1 & \sin\theta_1 \\ -\sin\theta_1 & \cos\theta_1 \end{bmatrix} \end{aligned} \tag{11}$$

Combined (1) and (11), the voltage in d-q coordinate system can be expressed as:

$$\begin{cases} u_{\mathrm{gd}} = u_{\mathrm{gd0}} + u_{\mathrm{gdsso}} \\ \approx U_{\mathrm{g}} + \sqrt{1+\Delta\theta^2}U_{\mathrm{sso}}\sin[(\omega_{\mathrm{sso}} - \omega_1)t \\ + (\varphi_{\mathrm{usso}} - \varphi_1 - \arctan\Delta\theta)] \\ u_{\mathrm{gq}} = u_{\mathrm{gq0}} + u_{\mathrm{gqsso}} \\ \approx -U_{\mathrm{g}}\Delta\theta + \sqrt{1+\Delta\theta^2}U_{\mathrm{sso}} \\ \sin[(\omega_{\mathrm{sso}} - \omega_1)t + (\varphi_{\mathrm{usso}} - \varphi_1 - \arctan\Delta\theta)] \end{cases} \tag{12}$$

The simulation in Fig. 4 is the voltage amplitude estimate of PLL under SSO state in the grid. The simulation results confirm that there is an oscillation component with frequency of $\omega_1 - \omega_{\mathrm{sso}}$ in the voltage amplitude estimation results of PLL output in the SSO state of the power grid, which also verifies the accuracy of (12)

Similarly, (2) can be further accurately expressed as (14), as shown at the bottom of the next page.

$$\begin{cases} i_{\mathrm{gd}} = I_{\mathrm{g}} + \sqrt{1+\Delta\theta^2}I_{\mathrm{sso}} \\ \sin[(\omega_{\mathrm{sso}} - \omega_1)t + \varphi_{\mathrm{isso}} - \varphi_1 + \arctan\dfrac{1}{\Delta\theta}] \\ i_{\mathrm{gq}} = -\Delta\theta \cdot I_{\mathrm{g}} + \sqrt{1+\Delta\theta^2}I_{\mathrm{sso}} \\ \sin[(\omega_{\mathrm{sso}} - \omega_1)t + \varphi_{\mathrm{isso}} - \varphi_1 + \arctan\dfrac{1}{\Delta\theta}] \end{cases} \tag{13}$$

At this time, the power expression of GSC considering the influence of PLL is (15), as shown at the bottom of the next page. In (14), $A = \sqrt{1+\Delta\theta^2}(1-\Delta\theta)(U_{\mathrm{g}}I_{\mathrm{sso}} + U_{\mathrm{sso}}I_{\mathrm{g}})$.

Equation (14) reflects the oscillation quantity of grid voltage and current coupling with $\Delta\theta$, which increases the complexity of GSC system oscillation modes. At this time, according to (14), the SSO component of the power grid acts on the GSC system, making the active power produce the AC component of frequency. At this time, the variation of the active power oscillation component P_{gsso} is affected by multiple factors such as the amplitude, frequency and phase angle of the secondary synchronous voltage. Therefore, when designing the oscillation power suppression strategy, it is necessary to make it able to effectively suppress the oscillation power even when the above three factors change.

D. ANALYSIS OF QUASI-RESONANT CONTROL EFFECT UNDER SSO VARIATION IN POWER GRID

It can be seen from the above analysis that the changes of SSO amplitude, frequency and phase Angle in the power grid have varying degrees of influence on the active power P_{g} of GSC. Therefore, the changes of the above factors should be considered when designing the suppression strategy of SSO.

In order to verify the impact of SSO characteristic changes on the designed oscillation suppression strategy, based on literature [25], the ω_0 of the quasi-resonant controller was set as 40Hz, and the relevant simulation analysis was performed on the GSC power oscillation suppression strategy based on the quasi-resonant controller when DFIG was running at the super-synchronous speed of 1800r/min. The parameters adopted in the simulation are shown in Table 2.

The simulation conditions are as follows: when the simulation runs to 3.0 s, the SSO voltage is put in, runs to 3.2 s, the quasi-resonant suppressor is added, runs to 3.5 s, the SSO characteristics change.

TABLE 2. Simulation related parameters.

Parameters	Value	Parameters	Value
rated power	2 MW	stator resistance	$2.6*10^{-3}\,\Omega$
stator voltage	690 V	stator leakage	$8.7*10^{-5}$ H
rated frequency	50 Hz	rotor resistance	$2.61*10^{-2}\,\Omega$
motor pole pairs	2	rotor leakage	$7.83*10^{-4}$ H
incoming inductance	$2*10^{-4}$ H	mutual Inductance	$2.5*10^{-3}$ H
DC bus capacitance	$2.88*10^{-2}$ F	DC side voltage	1500 V

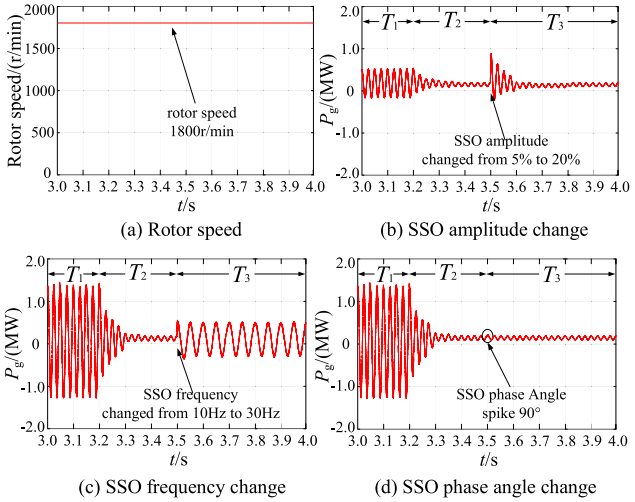

FIGURE 5. Suppression effect of quasi-resonant controller under SSO characteristic variation.

According to the simulation in Fig. 5, the oscillation component of the active power in the GSC system decreases significantly during the T_2 period. In Fig. 5(b), the SSO amplitude of the grid in T_3 period changes from 5% of the fundamental wave voltage to 20%, and the P_g oscillation amplitude increases instantaneously. However, after the adjustment of the quasi-resonant controller, the oscillation component of the GSC system is still effectively suppressed. In Fig. 5(c), the frequency of SSO in the grid during T_3 period changes from 10 Hz to 30 Hz, and the oscillation frequency of P_g occurs at 20 Hz. According to the results, the suppression strategy fails at this time, and P_g in the GSC system will maintain oscillation. In Fig. 5(d), the SSO phase angle of the grid changes suddenly during T_3 period. The simulation results in Fig. 5(d) confirm that the quasi-resonant controller can still effectively suppress the oscillation component in P_g, which proves that the phase angle has little influence on the control strategy.

III. RESEARCH ON THE SUPPRESSION METHOD OF PLL ESTIMATION ERROR UNDER THE INFLUENCE OF GRID SSO

A. SSO SUPPRESSOR BASED ON RESONANT CONTROLLER

According to the above analysis, when there is SSO voltage with a frequency of ω_{sso} in the power grid, the working performance of the PLL will be interfered by oscillating voltage, which will affect the stability of the GSC control strategy. It also increases the complexity of P_g oscillations in GSC. Therefore, in order to eliminate the errors in PLL output estimates in the SSO state of the power grid, it is necessary to design corresponding suppression strategies to ensure the accuracy of the PLL operation.

In the AC component control, the resonant controller is often used. Therefore, a resonant controller is also considered in this paper to suppress the input oscillation voltage to the PLL. The transfer function of the resonant controller is as follows [26]:

$$G_1(s) = \frac{K_R s}{s^2 + \omega_0^2} \tag{16}$$

In (16), K_R is the gain coefficient of resonance control; ω_0 is the resonant frequency.

In order to further verify the working characteristics of (16), Bode diagram is used for corresponding analysis and discussion. The ω_0 of the resonant controller is set as 50 Hz, and when K_R changes, the amplitude-frequency and phase-frequency diagrams of the resonant controller shown in (16) are shown in Fig. 6.

$$\begin{aligned} P_g &= -\frac{3}{2}(u_{gd}^* i_{gd} + u_{gq}^* i_{gq}) \\ &= -\frac{3}{2}\begin{bmatrix} (u_{gd0} + u_{gd1} + u_{gd2} + u_{gd3})^*(i_{gd0} + i_{gd1} + i_{gd2} + i_{gd3}) \\ +(u_{gq0} + u_{gq1} + u_{gq2} + u_{gq3})^*(i_{gq0} + i_{gq1} + i_{gq2} + i_{gq3}) \end{bmatrix} \\ &\approx -\frac{3}{2}\begin{pmatrix} U_g I_g + \Delta\theta^2 U_g I_g + (1 + \Delta\theta^2) U_{sso} I_{sso} \\ +A\sin[(\omega_{sso} - \omega_1)t + \varphi_{usso} - \arctan\Delta\theta] \end{pmatrix} \end{aligned} \tag{14}$$

$$\begin{aligned} Q_g &= -\frac{3}{2}(u_{gq}^* i_{gd} - u_{gd}^* i_{gq}) \\ &= -\frac{3}{2}\begin{bmatrix} (u_{gq0} + u_{gq1} + u_{gq2} + u_{gq3})^*(i_{gd0} + i_{gd1} + i_{gd2} + i_{gd3}) \\ -(u_{gd0} + u_{gd1} + u_{gd2} + u_{gd3})^*(i_{gq0} + i_{gq1} + i_{gq2} + i_{gq3}) \end{bmatrix} \approx 0 \end{aligned} \tag{15}$$

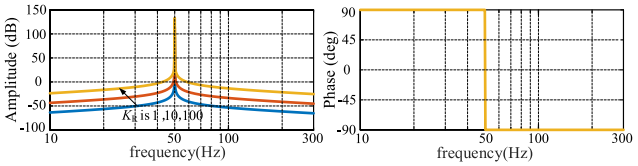

(a) Amplitude frequency characteristic (b) Phase frequency characteristic

FIGURE 6. Bode diagram analysis of resonant controller.

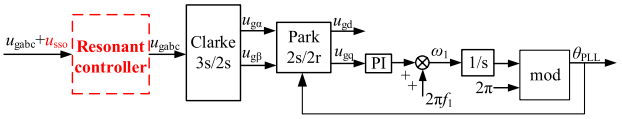

FIGURE 7. Improved PLL of series resonant controller.

The simulation results in Fig. 6 show that the resonant controller shown in (16) has extremely high gain only at the resonant frequency, and its gain is positively correlated with the gain coefficient K_R of the resonant control. Since the resonant controller only controls the signal with the same frequency as the resonant frequency, it can be considered to filter out the sub-synchronous component input to the PLL by taking full advantage of this characteristic.

B. RESEARCH ON IMPROVING PLL CONTROL STRATEGY IN SSO STATE

When the power grid voltage contains SSO component, the voltage estimated amplitude, angular velocity estimated value and phase estimated value of PLL output all have errors, resulting in PLL's difficulty in meeting the requirements of vector control in terms of phase locking accuracy and affecting the accuracy of control strategy. Therefore, PLL needs to be improved.

Based on the above analysis of the operating characteristics of the resonant controller, a resonant controller with a resonant frequency of 50Hz is connected in series at the input end of the PLL, so that only power frequency signals are allowed to enter the PLL, so as to avoid the influence of oscillating voltage on the PLL, so as to ensure the accuracy of the PLL. The improved PLL shown in Figure 7.

In order to verify the performance of the designed improved PLL in the SSO state of the power grid, the estimated output values of the improved PLL and the traditional PLL were compared and analyzed in the SSO state of the power grid. In the simulation process, the power grid voltage was 690 V and the frequency was 50 Hz. At 1.5 s, SSO voltage with the fundamental wave voltage amplitude of 20% and the frequency of 20 Hz was added. The simulation results are shown in Figure 8.

By observing Fig. 8(a) and (b), it can be seen that compared with the traditional PLL, the voltage fluctuation amplitude of the improved PLL of the proposed series resonance controller is significantly reduced in the d-q coordinate system. The simulation results in Fig. 8 show that the proposed improved PLL can accurately lock the fundamental voltage of the grid,

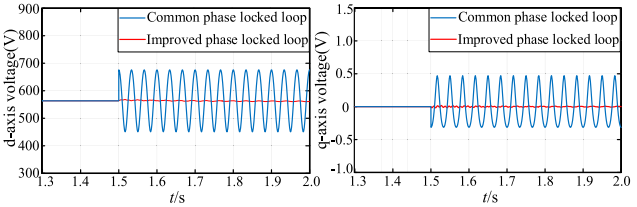

(a) d-axis voltage waveform (b) q-axis voltage waveform

FIGURE 8. Improved PLL simulation effect.

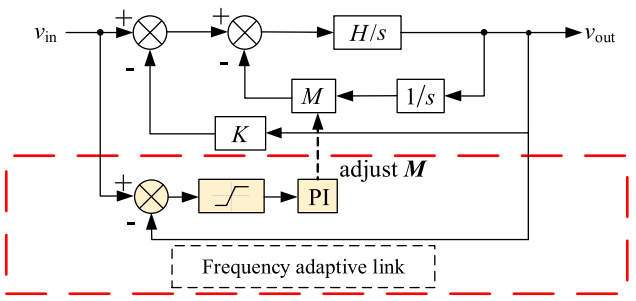

FIGURE 9. Adaptive quasi-resonant control structure.

thus avoiding the adverse influence of PLL errors on the control strategy of the GSC system. At the same time, the complexity of GSC power oscillation can be reduced.

IV. DFIG-GSC POWER OSCILLATION SUPPRESSION STRATEGY BASED ON ADAPTIVE QUASI-RESONANT CONTROLLER

A. DESIGN OF SUB-SYNCHRONOUS OSCILLATION SUPPRESSOR BASED ON ADAPTIVE QUASI-RESONANT CONTROLLER

According to the analysis in Section II-D above, it is clear that SSO frequency variation has the most significant effect on the oscillation suppression strategy based on the quasi-resonant controller. Therefore, a frequency adaptive algorithm is designed in this paper to change the resonant frequency of the quasi-resonant controller in real time, so as to suppress the power oscillation of the GSC system.

The transfer function of the quasi-resonant controller is shown below [27]:

$$G_2(s) = \frac{2K_R\omega_c s}{s^2 + 2\omega_c s + \omega_0^2} \tag{17}$$

In (17), ω_c represents cutoff frequency.

By transforming (17), we can obtain:

$$G_3(s) = \frac{Hs}{s^2 + HKs + MH} \tag{18}$$

In (18), $H = 2K_R\omega_c$ $K = \frac{1}{K_R}$ $M = \frac{\omega_0^2}{2K_R\omega_c}$.

According to (18), ω_0 is directly related to M, and the ω_0 can be controlled by adjusting M. The adaptive quasi-resonant controller designed according to (18) is shown in Fig. 9.

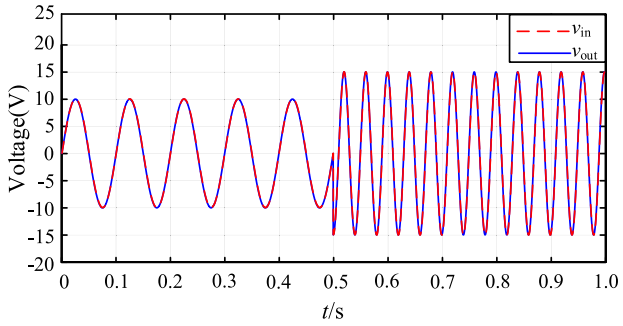

FIGURE 10. The effect diagram of the adaptive quasi-resonant controller when the input signal changes.

Set the input signal of the adaptive quasi-resonant controller shown in Fig. 9 as $v_{in} = A\sin(\omega_0 t)$. At this time, in order to realize the tracking of input signals, combined with (18), the output v_{out} can be expressed as:

$$v_{out} = A\,|G_3(j\omega)|\,\sin(\omega_0 t + \angle G(j\omega)) \tag{19}$$

In (19):
$$\begin{cases} \angle G_3(j\omega) = \dfrac{\pi}{2} - \arctan\dfrac{HK\omega_0}{MH - \omega_0^2} \\ |G_3(j\omega)| = \dfrac{H\omega_0}{\sqrt{(MH - \omega_0^2)^2 + (HK\omega_0)^2}} \end{cases}.$$

According to Fig. 9 and (19), when the resonant frequency of the quasi-resonant controller is ω_0, if the input signal frequency is also ω_0, then the output signal $v_{out} = (A/K)\sin(\omega_0 t)$. Let $K = 1$, then the input and output signals are the same. When the frequency of vin changes abruptly, the relationship between v_{in} and v_{out} can be approximately linear in a small range centered on the zero crossing of v_{out} due to the existence of the limiting value, and the parameter M can be changed through PI controller. Therefore, the difference between v_{in} and v_{out} can be utilized for real-time adaptive adjustment of M, so as to achieve the purpose of changing the resonant frequency of the quasi-resonant controller in quasi-real time [28].

The simulation of the adaptive quasi-resonant controller was built according to Fig. 9, and $K = 1$ and $H = 100$ were set. The initial resonant angular frequency ω_0 is 10 Hz. The control effect of the adaptive quasi-resonant controller is shown in Fig. 10 below:

As shown in Fig. 10, the original input voltage amplitude is 10 V and frequency is 10 Hz. At 0.5 s, the input voltage amplitude, frequency and phase all change. At this time, the parameter M of the adaptive quasi-resonant controller will change, and the input voltage signal tracking with variable frequency, amplitude and phase will be completed.

B. SUPPRESSION STRATEGY OF GSC POWER OSCILLATION IN SSO WITH PLL INFLUENCE

Based on the above theoretical research and simulation analysis, this paper proposes a DFIG-GSC power suppression strategy based on an adaptive quasi-resonant controller, as shown in Fig.11.

In Fig. 11, DFIG-GSC power oscillation suppression strategies include: ① is improved PLL structure; ② is the GSC's main circuit topology; ③ is the GSC's main circuit power calculation unit; ④ is DFIG-GSC power oscillation suppression strategy based on adaptive quasi-resonant control.

According to Fig. 11, after the improved PLL is applied to the GSC system, the phase required by the coordinate transformation process in its control strategy is an accurate phase because it can accurately lock the fundamental wave voltage of the power grid. At the same time, the feedforward decoupling oscillation in the control strategy is significantly reduced, and the complexity of GSC power calculation is also reduced.

Aiming at the power oscillation component in the GSC system, an adaptive quasi-resonant controller is used to suppress it. The process is as follows:

There is no SSO component in the power grid, and there is no oscillation component in the GSC system during stable operation. The two control objectives of the GSC are to maintain the V_{dc} voltage stability of the DC bus and to maintain the power factor of the converter is 1. In this case, the active power of the GSC system is the fundamental direct flow. The adaptive quasi-resonant controller has no control over the DC component, that is, the output of v_{d2} is 0. In this case, the above goals can be achieved using only the PI controller.

When SSO exists in the grid, the grid side voltage and current both contain sub-synchronous components. According to (14), at this time, the active power P_g flowing through the grid side of GSC will produce corresponding oscillation. Because the oscillation is AC and the amplitude of oscillation is high, the PI controller cannot realize the tracking control of the sub-synchronous component only.

When SSO component exists in the power grid, there is a certain oscillation component in the grid side voltage and current. At the time, according to (14), the grid side active power P_g flowing through GSC will produce corresponding oscillation. In addition, according to the above simulation, the amplitude of power oscillation is high, and the PI controller alone cannot effectively control the sub-synchronous component.

In this paper, an adaptive quasi-resonant controller is designed to suppress the oscillating power in the GSC system. Specifically, the difference between the reference value and the actual value of the active power oscillation of the GSC system is used as the input signal of the adaptive quasi-resonant controller, and the sub-synchronous component of the input signal is tracked in real time using the adaptive algorithm shown in Fig. 9. The output voltage v_{d2} of the adaptive quasi-resonant controller is used as the voltage to suppress the active power oscillation. Combined with the control voltage v_{d1} generated by the PI controller, the oscillation component in P_g can be finally suppressed by controlling the current of GSC.

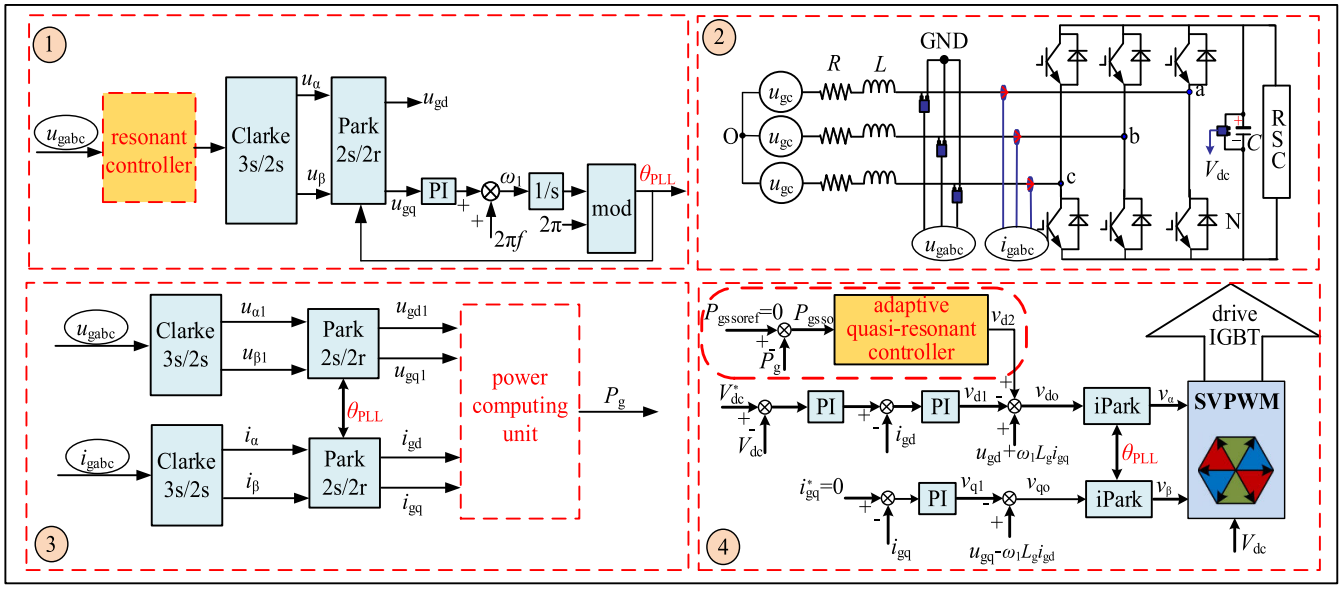

FIGURE 11. DFIG-GSC power oscillation suppression strategy based on adaptive quasi resonator.

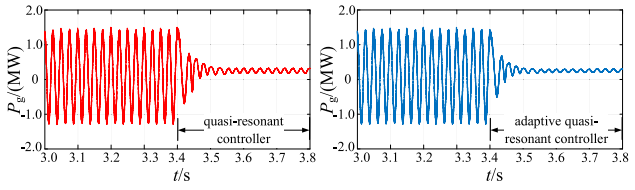

(a) Quasi-resonant control (b) Adaptive quasi-resonant control

FIGURE 12. Oscillation suppression diagram of power grid SSO frequency 10 Hz.

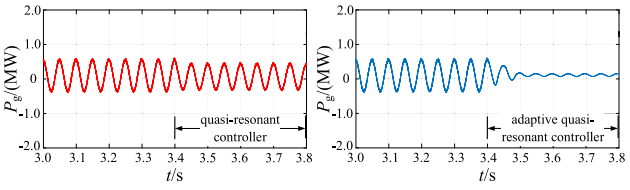

(a) Quasi-resonant control (b) Adaptive quasi-resonant control

FIGURE 13. Oscillation suppression diagram of power grid SSO frequency 30 Hz.

The adaptive quasi-resonant controller can effectively suppress the active power oscillation of the GSC system when SSO occurs and improve the stability of the GSC system.

V. SIMULATION ANALYSIS AND EXPERIMENTAL VERIFICATION

A. SIMULATION ANALYSIS

In this paper, a DFIG-GSC P_g oscillation suppression strategy based on an adaptive quasi-resonant controller is proposed, and the suppression effect of the aligning resonant controller and the adaptive quasi-resonant controller on the GSC power oscillation is compared under the condition of 1800r/min.

The simulation conditions are as follows: in the SSO state of the power grid, two controllers are put in when running to 3.4 s, and the resonant frequency is set as 40 Hz, and the SSO voltage amplitude is 20% of the fundamental wave voltage amplitude.

The simulation results in Fig. 12 to Fig. 13 show that the quasi-resonant controller can only suppress the oscillation component when the SSO frequency is 10 Hz, and the suppression effect is not good for the oscillation component when the SSO frequency is 30 Hz. The simulation in Fig. 12(d) and Fig. 13(d) shows that SSO frequency change has no influence on the suppression effect of the adaptive quasi-resonant controller, and can effectively suppress the oscillation power of GSC.

TABLE 3. DFIG experimental platform related parameters.

Parameters	Value	Parameters	Value
rated power	15 kW	stator resistance	$3.79*10^{-1}\ \Omega$
stator voltage	200 V	stator leakage	$1.1*10^{-3}$ H
rated frequency	50 Hz	rotor resistance	$3.14*10^{-1}\ \Omega$
motor pole pairs	3	rotor leakage	$2.2*10^{-3}$ H
incoming inductance	$5*10^{-3}$ H	mutual Inductance	$4.27*10^{-2}$ H
DC bus capacitance	$2.2*10^{-3}$ F	DC side voltage	400 V

B. EXPERIMENTAL VERIFICATION

To verify the effectiveness of the proposed suppression strategy, a 15 kw DFIG system vibration suppression experiment platform was built. Parameters of the experimental platform are shown in Table 3.

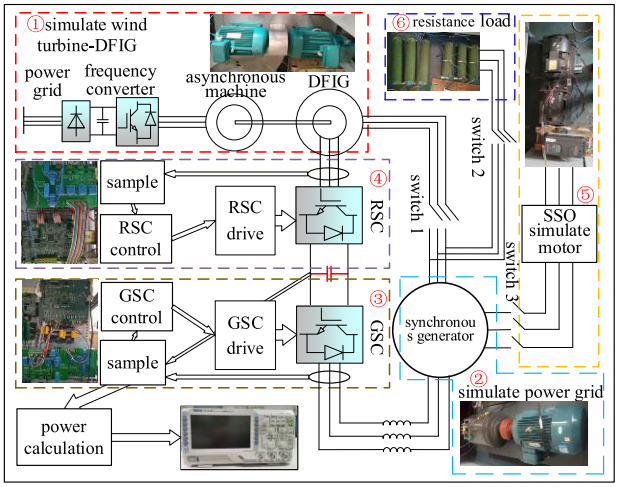

FIGURE 14. DFIG grid-connected system oscillation suppression experimental platform.

According to the DFIG grid-connected system oscillation suppression experimental platform shown in Fig. 14, it is seen that the platform consists of six parts, which are ① is simulate wind turbine-DFIG system, ② is simulate power grid, ③ is GSC control system, ④ is RSC control system, ⑤ is SSO simulate system, ⑥ is variable resistance load.

The simulate wind turbine is generated by driving the asynchronous motor by the frequency converter. The rotor of the asynchronous motor is connected with the rotor of DFIG. Simulate power grid is generated by synchronous motor; DSP28335 is used as the control chip of GSC and RSC. The SSO simulation system is generated by another synchronous motor whose output voltage is regulated by a frequency converter so that oscillating voltages of any frequency can be simulated.

Before experimental verification, it is necessary to verify whether the built experimental platform meets the requirements of grid connection. Before grid-connection, A-phase voltage of DFIG stator and A-phase voltage waveform of analog grid are shown in Fig. 15. As can be seen from Fig. 15, the three elements of DFIG stator voltage and grid voltage as well as the phase sequence are the same. Therefore, the experimental platform built has grid-connection conditions and can be grid-connected.

In the process of SSO suppression experiment of DFIG-GSC system, the stator output power of DFIG was set to 5 kW, the speed was set to 1200 r/min, and the voltage amplitude of SSO was set to 20% of the voltage amplitude of the analog grid, the frequencies were respectively 10 Hz and 30 Hz, and the resonant frequency of the two controllers was 40 Hz. The experimental results are shown in Fig. 16∼17.

Through the experimental results in Fig. 16∼17, it can be seen that consistent with the aforementioned simulation analysis, the quasi-resonant controller can only suppress the oscillation components with the same resonant frequency, while the adaptive quasi-resonant controller can effectively suppress the active power oscillation of GSC at different frequencies.

Finally, the effectiveness of the proposed oscillation suppression strategy is verified when SSO frequency changes. The experimental results are shown in Fig. 18.

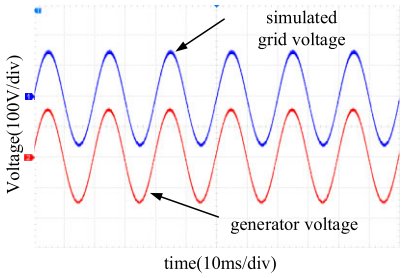

FIGURE 15. DFIG stator A-phase voltage and analog grid A-phase voltage waveform before grid-connection.

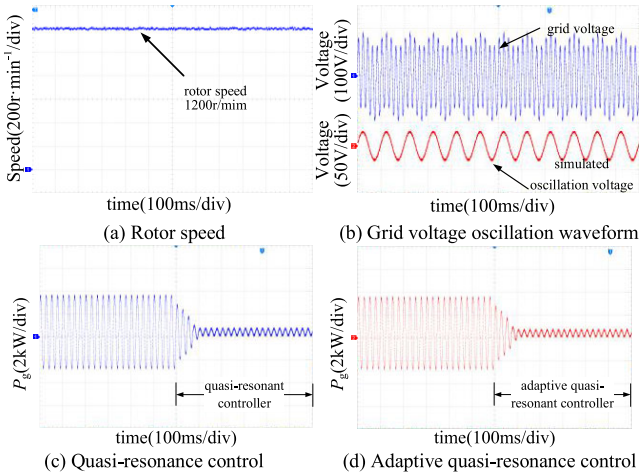

FIGURE 16. Effect diagram of oscillation suppression when SSO frequency of power grid is 10 Hz.

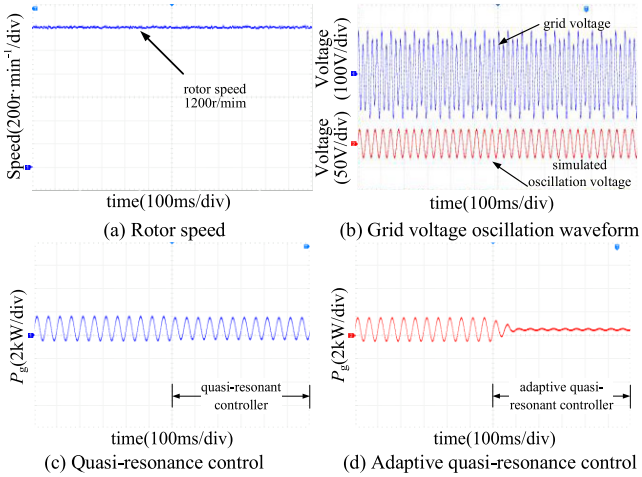

FIGURE 17. Effect diagram of oscillation suppression when SSO frequency of power grid is 30 Hz.

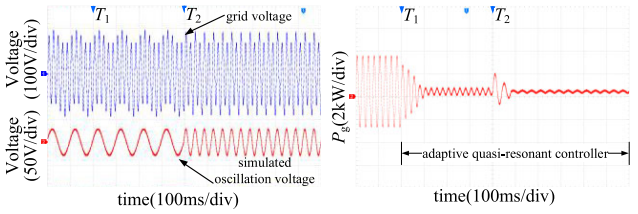

(a) Grid voltage oscillation waveform (b) GSC output P_g

FIGURE 18. The suppression effect of adaptive quasi-resonant controller on variable frequency oscillation.

In Fig. 18(a), the initial frequency of SSO voltage is 10 Hz, and the amplitude is 20% of the analog grid voltage. An adaptive quasi-resonant controller was put in at T_1 to suppress the GSC power oscillation. By observing $P_g$waveform in Fig. 18(b), it can be seen that the oscillation component of P_g is significantly weakened after the adaptive quasi-resonant controller is put into operation. The SSO frequency changed at T_2, and the oscillatory component in P_g was suppressed after 90 ms of adjustment time. The experiment proves the effectiveness of the strategy mentioned in this paper.

VI. CONSLUSION

In this paper, the influence of grid SSO on GSC output power quality is studied. Considering the interference of PLL on GSC system and the influence of SSO frequency change aligning resonance suppression strategy, a measure is proposed to suppress the sub-synchronous component of GSC system and improve its output power quality. In order to improve the accuracy of the estimated output value of PLL, a control strategy based on adaptive quasi-resonant controller is proposed to suppress the active power oscillation of GSC system. The conclusion are as follows:

(1) The improved PLL can accurately lock the fundamental voltage signal of power grid, so as to eliminate a series of adverse disturbances caused by the output error of PLL estimation, and effectively reduce the oscillation component of the current loop feedback and feedforward decoupling compensation. At the same time, the complexity of GSC power calculation is reduced.

(2) The simulation results show that the variation of SSO frequency has great influence on the suppression effect of quasi-resonant controller. To solve this problem, an adaptive algorithm is proposed to improve the quasi-resonant controller to suppress the oscillatory component in the active power of GSC.

(3) Through simulation and experimental verification, the DFIG-GSC oscillation suppression strategy designed in this paper can effectively realize the purpose of suppressing the oscillation component of the active power in the GSC system, and can still quickly achieve the suppression effect when the SSO frequency changes, and improve the power quality of the output of GSC.

This paper is one of the series of articles on improving the stability of new energy power generation systems. In the future research, we will focus on the stability of new energy power generation systems under the fault phenomena of DFIG integral unit, permanent magnet direct drive generator set, photovoltaic and so on, including but not limited to SSO, unbalanced voltage of grid and so on.

REFERENCES

[1] S. Puchalapalli and B. Singh, "A novel control scheme for wind turbine driven DFIG interfaced to utility grid," *IEEE Trans. Ind. Appl.*, vol. 56, no. 3, pp. 2925–2937, May 2020.

[2] J. Ma and Y. Shen, "Stability assessment of DFIG subsynchronous oscillation based on energy dissipation intensity analysis," *IEEE Trans. Power Electron.*, vol. 35, no. 8, pp. 8074–8087, Aug. 2020.

[3] H. Dong, M. Su, K. Liu, and W. Zou, "Mitigation strategy of subsynchronous oscillation based on fractional-order sliding mode control for VSC-MTDC systems with DFIG-based wind farm access," *IEEE Access*, vol. 8, pp. 209242–209250, 2020.

[4] M. Abdeen, S. H. A. El-Banna, S. Elgohary, H. Mostafa, N. Ghaly, N. Adel, Z. Elkhwas, M. Alahmady, H. M. Zawbaa, and S. Kamel, "Adaptive fuzzy supplementary controller for SSR damping in a series-compensated DFIG-based wind farm," *IEEE Access*, vol. 11, pp. 1467–1476, 2023.

[5] L. Zhu, D. Zhong, B. Wang, R. Lin, and M. Xu, "Understanding subsynchronous oscillation in DFIG-based wind farms with rotor-side converter control based on the equivalent RLC model," *IEEE Access*, vol. 8, pp. 65371–65382, 2020.

[6] L. Chen, S. Xu, H. Sun, T. Bi, R. Song, J. Yi, and Q. Guo, "A survey on wide-frequency oscillation for power systems with high penetration of power electronics," *Proc. CSEE*, vol. 41, no. 7, pp. 2297–2310, Apr. 2021.

[7] D. Fateh, A. A. M. Birjandi, and J. M. Guerrero, "Safe sub synchronous oscillations response for large DFIG-based wind farms," *IEEE Access*, vol. 8, pp. 169822–169834, 2020.

[8] H. Sun, T. Xu, Q. Guo, Y. Li, W. Lin, J. Yi, and W. Li, "Analysis on blackout in Great Britain power grid on August 9th 2019 and its enlightenment to power grid in China," *Proc. CSEE*, vol. 39, no. 21, pp. 6183–6192, Nov. 2019.

[9] W. Wang, C. Zhang, G. He, G. Li, J. Zhang, and H. Wang, "Overview of research on subsynchronous oscillations in large-scale wind farm integrated system," *Power Syst. Technol.*, vol. 41, no. 4, pp. 1050–1060, Apr. 2017.

[10] X. Xie, L. Wang, J. He, H. Liu, C. Wang, and Y. Zhan, "Analysis of subsynchronous resonance/oscillation types in power systems," *Power Syst. Technol.*, vol. 41, no. 4, pp. 1043–1049, Apr. 2017.

[11] G. F. Gontijo, T. C. Tricarico, L. F. da Silva, D. Krejci, B. W. França, M. Aredes, and J. M. Guerrero, "Modeling, control, and experimental verification of a DFIG with a series-grid-side converter with voltage sag, unbalance, and distortion compensation capabilities," *IEEE Trans. Ind. Appl.*, vol. 56, no. 1, pp. 584–600, Jan. 2020.

[12] B. Pang and H. Nian, "Collaborative control and allocation method of RSC and GSC for DFIG system to suppress high-frequency resonance and harmonics," *IEEE Trans. Ind. Electron.*, vol. 67, no. 12, pp. 10509–10519, Dec. 2020.

[13] Y. He and J. Hu, "Several hot-spot issues associated with the grid-connected operations of wind-turbine driven doubly fed induction generators," *Proc. CSEE*, vol. 32, no. 27, pp. 1–15, Sep. 2012.

[14] H. Li, "Research on control strategy of DFIG grid-connected inverter under grid voltage distortion," M.S. thesis, Dept. Elect. Eng., Harbin Inst. Technol., Harbin, China, 2017.

[15] B. Zhou, Y. Song, H. Nian, and C. Cheng, "Improved direct power control strategy of DFIG system under unbalanced and distorted grid voltage," *Trans. China Electrotech. Soc.*, vol. 32, no. 24, pp. 233–243, Dec. 2017.

[16] H. Yang, "Research on control strategy of doubly-fed induction generator under unbalanced grid voltage," M.S. thesis, Dept. Elect. Eng., Hefei Univ. Technol., Hefei, China, 2017.

[17] X. Yang, "Model predictive control of DFIG under unbalanced grid voltage conditions," M.S. thesis, Dept. Elect. Eng., Taiyuan Univ. Technol., Taiyuan, China, 2021.

[18] X. Yan, W. Chang, S. Cui, Y. Sun, and J. Jia, "Sub-synchronous oscillation suppression strategy of weak AC wind power system with static VAR compensator based on linear active disturbance rejection control," *Trans. China Electrotech. Soc.*, vol. 37, no. 11, pp. 2825–2836, Aug. 2021.

[19] H. A. Mohammadpour and E. Santi, "Optimal adaptive sub-synchronous resonance damping controller for a series-compensated doubly-fed induction generator-based wind farm," *IET Renew. Power Gener.*, vol. 9, no. 6, pp. 669–681, Aug. 2015.
[20] X. Tian, Y. Chi, Y. Li, H. Tang, C. Liu, and Y. Su, "Coordinated damping optimization control of sub-synchronous oscillation for DFIG and SVG," *CSEE J. Power Energy Syst.*, vol. 7, no. 1, pp. 140–149, Jan. 2021.
[21] I. Vieto and J. Sun, "Damping of subsynchronous resonance involving type-III wind turbines," in *Proc. IEEE 16th Workshop Control Modeling Power Electron. (COMPEL)*, Vancouver, BC, Canada, Jul. 2015, pp. 1–8.
[22] B. Gao, Y. Hu, R. Li, L. Yao, and S. Zhao, "Research on subsynchronous control interaction mitigation strategy based on active disturbance rejection control for doubly-fed induction generator," *Power Syst. Technol.*, vol. 43, no. 2, pp. 655–664, Sep. 2019.
[23] X. Wu, M. Wang, M. Shahidehpour, S. Feng, and X. Chen, "Model-free adaptive control of STATCOM for SSO mitigation in DFIG-based wind farm," *IEEE Trans. Power Syst.*, vol. 36, no. 6, pp. 5282–5293, Nov. 2021.
[24] C. Hong, "Analysis of sub-synchronous oscillation characteristics of doubly-fed wind farm and research on multi-turbine cooperative mitigation strategy," M.S. thesis, Dept. Elect. Eng., North China Electr. Power Univ., Beijing, China, 2021.
[25] F. Meng, D. Sun, K. Zhou, J. Wu, F. Zhao, and L. Sun, "A sub-synchronous oscillation suppression strategy for doubly fed wind power generation system," *IEEE Access*, vol. 9, pp. 83482–83498, 2021.
[26] Z. Wang, Z. Pan, and Z. Xu, "Control strategy of island effect of double-fed wind turbine with nonlinear loads," *Acta Energiae Solaris Sinica*, vol. 36, no. 8, pp. 1791–1798, 2015.
[27] H. Chuan, S. M. Fazeli, Z. Wu, and R. Burke, "Mitigating the torque ripple in electric traction using proportional integral resonant controller," *IEEE Trans. Veh. Technol.*, vol. 69, no. 10, pp. 10820–10831, Oct. 2020.
[28] H. Yang, G. Song, F. Teng, H. Li, and Y. Chen, "Adaptive proportional complex integral control strategy for single-phase grid-connected inverter," *High Voltage Eng.*, vol. 46, no. 11, pp. 3790–3799, Nov. 2021.

DONGYANG SUN received the B.S. and M.S. degrees in electrical engineering from the Harbin University of Science and Technology, Harbin, China, in 2010 and 2014, respectively, and the Ph.D. degree in electrical engineering from the Harbin Institute of Technology (HIT), Harbin, in 2019.

He is currently an Associate Professor with the Harbin University of Science and Technology. His research interests include power electronics, modeling, control and energy management, and high-power converters for distributed power systems.

WENQIANG SHEN received the B.S. degree in electrical engineering from Shandong Technology and Business University, Yantai, China, in 2021. He is currently pursuing the master's degree with the Harbin University of Science and Technology. His research interest includes the stability of new energy power generation.

ZIJIE QIAN received the B.S. degree in electrical engineering from Jiangsu University, Zhenjiang, China, in 2022. He is currently pursuing the master's degree with the Harbin University of Science and Technology. His research interests include wind power system stability, power electronics, modeling, and control.

FANYI MENG received the B.S. degree in electrical engineering from China Three Gorges University, Yichang, China, in 2020. He is currently pursuing the master's degree with the Harbin University of Science and Technology. His research interests include power electronics, modeling, and control.

YUTONG SHA received the B.S. degree in electrical engineering from the Harbin University of Science and Technology Rongcheng Campus, Weihai, China, in 2021. She is currently pursuing the master's degree with the Harbin University of Science and Technology. Her research interests include wind and photovoltaic power system stability.

KAI ZHOU received the B.S. degree in communication engineering from Qiqihar University, Qiqihar, China, in 2006, and the M.S. and Ph.D. degrees in electrical engineering from the Harbin University of Science and Technology, Harbin, China, in 2009 and 2012, respectively.

He is currently a Professor with the Harbin University of Science and Technology. His research interests include automotive electronics, motor control, and new energy vehicles.